Bioactive Materials 6 (2021) 529–542

Contents lists available at ScienceDirect

Bioactive Materials

journal homepage: http://www.keaipublishing.com/biomat

Macrophage membrane-coated nanocarriers Co-Modified by RVG29 and TPP improve brain neuronal mitochondria-targeting and therapeutic efficacy in Alzheimer's disease mice

Yang Han[a,b], Chunhong Gao[b], Hao Wang[b], Jiejie Sun[b], Meng Liang[b], Ye Feng[b], Qianqian Liu[b], Shiyao Fu[b], Lin Cui[b], Chunsheng Gao[b], Yi Li[b,*], Yang Yang[b,**], Baoshan Sun[c,d,***]

[a] School of Traditional Chinese Medicine, Shenyang Pharmaceutical University, Shenyang, 110016, PR China
[b] State Key Laboratory of Toxicology and Medical Countermeasures, Beijing Institute of Pharmacology and Toxicology, Beijing, 100850, PR China
[c] School of Functional Food and Wine, Shenyang Pharmaceutical University, Shenyang, 10016, PR China
[d] Instituto National de Investigação Agrária e Veterinária, I.P., Pólo Dois Portos, Quinta da Almoinha, Dois Portos, 2565-191, Portugal

ARTICLE INFO

Keywords:
Macrophage-membrane coating
Biomimetic nanosystems
Neuronal mitochondria targeting
Blood-brain barrier
Alzheimer's disease
Genistein

ABSTRACT

Neuronal mitochondrial dysfunction caused by excessive reactive oxygen species (ROS) is an early event of sporadic Alzheimer's disease (AD), and considered to be a key pathologic factor in the progression of AD. The targeted delivery of the antioxidants to mitochondria of injured neurons in brain is a promising therapeutic strategy for AD. A safe and effective drug delivery system (DDS) which is able to cross the blood-brain barrier (BBB) and target neuronal mitochondria is necessary. Recently, bioactive materials-based DDS has been widely investigated for the treatment of AD. Herein, we developed macrophage (MA) membrane-coated solid lipid nanoparticles (SLNs) by attaching rabies virus glycoprotein (RVG29) and triphenylphosphine cation (TPP) molecules to the surface of MA membrane (RVG/TPP-MASLNs) for functional antioxidant delivery to neuronal mitochondria. According to the results, MA membranes camouflaged the SLNs from being eliminated by RES-rich organs by inheriting the immunological characteristics of macrophages. The unique properties of the DDS after decoration with RVG29 on the surface was demonstrated by the ability to cross the BBB and the selective targeting to neurons. After entering the neurons in CNS, TPP further lead the DDS to mitochondria driven by electric charge. The Genistein (GS)- encapsulated DDS (RVG/TPP-MASLNs-GS) exhibited the most favorable effects on reliveing AD symptoms *in vitro* and *in vivo* by the synergies gained from the combination of MA membranes, RVG29 and TPP. These results demonstrated a promising therapeutic candidate for delaying the progression of AD via neuronal mitochondria-targeted delivery by the designed biomimetic nanosystems.

1. Introduction

Alzheimer's disease (AD) is a kind of persistent neurological disorder with slow onset and worsening over time. At present, a large number of drug developments and clinical researches on AD treatment are carried out with beta-amyloids (aβ) as the target. Increasing evidences have confirmed that mitochondrial dysfunction is an early event of AD [1–3]. Simultaneously, oxidative stress of neuron mitochondria is closely related to the production and aggregation of Aβ. It has been shown that oxidative stress of neuron mitochondria leads to the production of Aβ [4], and the increase and aggregation of Aβ will further aggravate oxidative stress and damage to mitochondria [5]. Although the brain only accounts for 2% of the body weight, it consumes 25% of the whole body oxygen. Mitochondria are the main subcellular organelles for oxygen utilization. Reactive oxygen species (ROS), as a by-product of mitochondrial oxidative phosphorylation, are more easily produced in the brain with higher oxygen consumption. However, the low ROS scavenging ability of brain neurons makes them more vulnerable to oxidative stress and injury [6,7]. It has also been confirmed that mitochondrial dificits appear earlier in neurons than in non neuronal cells [8]. The abnormal function of mitochondria and the aggregation of aβ will lead to the apoptosis of neurons lacking

Peer review under responsibility of KeAi Communications Co., Ltd.
* Corresponding author.
** Corresponding author.
*** Corresponding author. School of Functional Food and Wine, Shenyang Pharmaceutical University, Shenyang, 10016, PR China.
E-mail addresses: liyi_evening@pku.edu.cn (Y. Li), amms2013@126.com (Y. Yang), sun.baoshan@iniav.pt (B. Sun).

https://doi.org/10.1016/j.bioactmat.2020.08.017
Received 21 May 2020; Received in revised form 21 August 2020; Accepted 23 August 2020

regeneration ability [9]. Recent studies have treated neuronal mitochondria dysfunction as a new therapeutic target for AD [10,11].

Several natural antioxidants have been used in the research of AD treatment. Genistein (GS), one of the most active natural flavonoids, exerts various biological effects including chemoprevention, antioxidation, anti-inflammatory and neuroprotection, shown to relieve AD symptoms. GS can effectively protect neuron apoptosis induced by aβ *in vitro* [12]. However, GS can only play a limited role in cognitive recovery and memory improvement *in vivo* [13]. This is attributed to its extremely poor aqueous solubility (5.3 μM), low oral bioavailability, poor brain accumulation and lack of mitochondrial targeting [14,15]. Pharmacokinetic studies showed most of GS were accumulated in stomach (1.83 μg/g), followed by intestine (1.50 μg/g), liver (1.13 μg/g), kidney (0.41 μg/g), lung (0.27 μg/g), heart (0.23 μg/g), and only 0.097 μg/g in brain at 6 h after oral dose of 12.5 mg/kg genistein in rats [15].

Nano DDS has attracted attention as a platform for delivery of therapeutic agents to targets. Importantly, appropriate modification enabled DDS to cross the blood-brain barrier and to deliver to the specifictarget in CNS. In addition to the main functions, features of prolonged circulation and good biocompatibility are also indispensable for DDS. However, it is a considerable challenge for a single nanosystem combining all of the above characteristics together. For example, a mitochondria-targeting Ceria nanoparticle administered via ipsilateral hippocampal stereotactic injection for AD therapy, for the reason of the poor ability to cross the BBB of the designed nanoparticles [16]. Additionally, biodegradation *in vivo* is a major challenge for inorganic materials-based nanoparticles [16]. Thus, it is limited for the designed nanocarriers themselves to be applied for AD therapy in clinic.

Recently, bioinspired strategies are gaining attention for drug delivery application because the nanoparticles are engineered to mimic the cellular functions, including erythrocytes, macrophages, leukocytes, tumor cells, and stem cells, etc [10,17–20]. Among them, erythrocytes membrane-coated nanocarriers have received much research attention for their long circulation half-life and low immunogenicity feature [21]. In addition, erythrocytes are the most readily available and abundant cells in body. However, the difference of blood group antigens expressed on the surface of erythrocyte membrane will lead to the strong rejection between erythrocytes. Thus, the biomimetic nanosystem prepared by the non homologous erythrocytes membrane may cause the abnormal immune response or heterogeneous immune response in the body of the subject. Macrophages as the key immune cells *in vivo*, have the natural ability to be recruited into the inflammatory area of the body. The innate inflammation-directed chemotactic ability could drive drug-loaded macrophages to accumulate in chronic inflammatory brain suffering from neurodegenerative diseases [22,23]. Meanwhile, various delivery vectors have been integrated into macrophage-membrane systems with prolonged systematic retention time, less reticuloendothelial system (RES) clearance, and reduced immunorecognition [24,25]. For the prevention and treatment of chronic neurodegenerative diseases, toxicity issue is another key aspect of drug delivery system. Solid lipid nanoparticles (SLNs) are one of various nanoparticles which based on natural lipids whose degradation products may not influence the extracellular/intracellular environment. In addition, production of SLNs, which needs no organic solvent, makes it one of the best choices for targeting brain neurodegenerative diseases [26].

Herein, we explored the use of MA membranes as a kind of bioactive material to camouflage SLNs (MASLNs) to improve the reticuloendothelial system (RES) evasion capability and to prolong the circulation of the nanosystems. The MA membranes isolated from c57BL/6J mice-derived peritoneal macrophages inherited the immunological characteristics of macrophages with high expression of F4/80 and CD11b, which may drive the biomimetic nanosystem to accumulate in AD brain with chronic inflammatory somewhat correlated with the innate inflammation-directed chemotactic ability. To strengthen the delivery efficiency for BBB-crossing and neuronal-targeting, RVG29 peptide isolated from rabies virus was decorated on the surface of MA membrane. Meanwhile, the modification of positively charged triphenylphosphine (TPP) ligand on the surface of MASLNs provided the mitochondrial-targeting property for the DDS by taking advantage of negative mitochondrial membrane potential [29]. Combining all the characteristics of MA membranes, RVG29 and TPP together, the designed biomimetic nanoparticles (RVG/TPP-MASLNs) were schematic prepared (Fig. 1A) and encapsulated with Genistein (GS) for the prevention of AD *in vitro* and *in vivo*. The present results provided a proof-of-concept evidence that the neuronal mitochondria-targeted delivery by the designed biomimetic nanosystems may have the potential as a promising strategic candidate for delaying the progression of AD.

2. Materials and methods

2.1. Materials

Amino-RVG29 and carboxy-TPP were provided by Xi'an ruixi Biological Technology Co., Ltd (Xi'an, China). Glycerol monostearate, Tween 80 and soya lecithin were provided by Fenglijingqiu Commerce and Trade Co., Ltd. (Beijing, China). Genistein was purchased from Sigma-Aldrich (USA). Anti-F4/80, anti-CD11b, anti-$A\beta_{1\text{-}42}$, anti-Iba1, anti-GFAP antibodies were purchased from Abcam (Cambridge, UK). Na,K-ATPase, β-Actin, GAPDH and anti-rabbit antibodies conjugated to horseradish peroxidase were from Cell Signaling Technology (MA, USA). 1,1′-Dioctadecyl-3,3,3′,3′-tetramethylindotricarbocyanine iodide (DIR) and coumarin-6 (Cou6) were purchased from Biotium. All chemicals were of reagent grade and were obtained from Sigma-Aldrich, unless otherwise stated.

2.2. Cell culture and animal experimentation

In accordance with previous report, mouse peritoneal macrophages [30] were isolated from c57BL/6 J mice. Astrocytes were isolated from 7-day Sprague–Dawley (SD) rats and maintained in Astrocyte Basal Medium-2 (iCell Bioscience Inc, Shanghai, China) [31]. Brain microvascular cell line (bEnd.3) was obtained from ATCC (Maryland, USA). HT22 cells were purchased from the iCell Bioscience Inc (shanghai, China). HT22 and bEnd.3 cells were maintained in culture medium consisting of dulbecco's modified eagle's medium (DMEM) supplemented with 10% FBS, 100 IU/mL penicillin, and 100 mg/mL streptomycin. The cells were maintained in a 37 °C humidified incubator in a 5% CO_2 atmosphere. HT22 cells were differentiated in NeuroBasal medium (Invitrogen, CA, USA) containing 1× N2 supplement (Gibco, CA, USA) for 48 h before use [32].

C57BL/6J mice and Sparague-Dawley rats were provided by Vital River Laboratories (Beijing, China). The APP/PS1 mice were obtained from Zhishan Healthcare Research Institute Ltd (Beijing, China). All animal experiments were complied with the code of ethics in research, training and testing of drugs issued by the Animal Care and Use Ethics Committee in Beijing Institute of Pharmacology and Toxicology.

2.3. Synthesis of functional conjugates

DSPE-PEG_{2000}-RVG29 was synthesized using an MAL-amino coupling reaction. Briefly, amino-RVG29 was dissolved in dimethylformamide (DMF) and added to DSPE-PEG_{2000}-MAL, at an amino-RVG29 to lipid molar ratio of 1.5: 1. The mixture was gently stirred overnight at room temperature in the dark. The resulting supernatant was dialyzed against distilled water for 48 h. The purified dialysate was lyophilized and stored at −20 °C. DSPE-PEG_{2000}-TPP was prepared using an NH_2-carboxy coupling reaction. Briefly, carboxy-TPP was reacted with DSPE-PEG_{2000}-NH_2 (1.5: 1 molar ratio) in chloroform containing EDC (1-(3-Dimethylaminopropyl)-3-ethylcarbodiimide hydrochloride) and NHS (N-Hydroxysuccinimide) (5 eq.) at room temperature for 12 h with gentle mixing. The reactants were then dialyzed in a dialysis bag to remove the organic solvent and unconjugated reactants. The solution

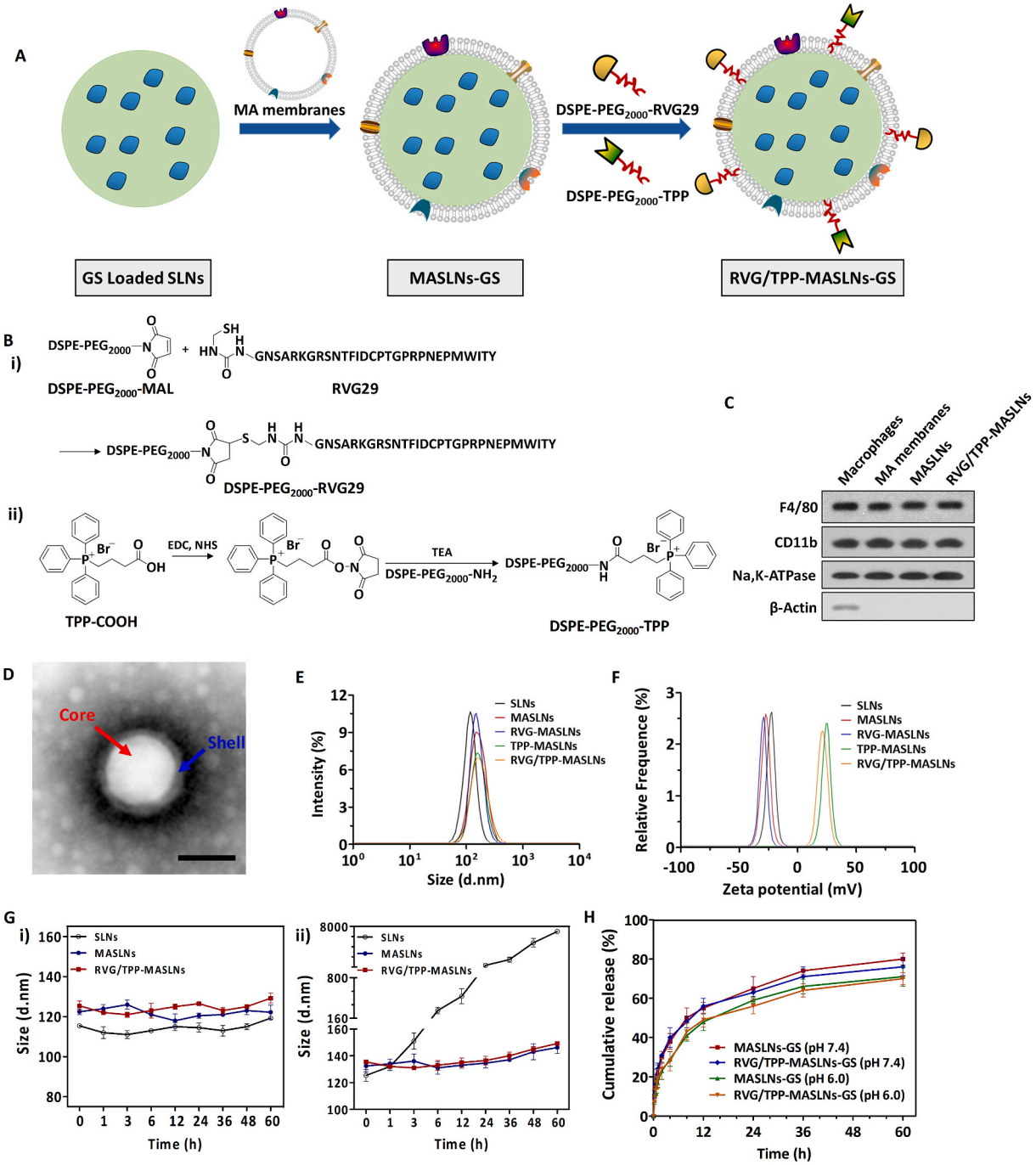

Fig. 1. Preparation and characterization of RVG/TPP-MASLNs-GS. (A) Schematic preparation of RVG/TPP-MASLNs-GS. (B) Principle of the preparation of (i) DSPE-PEG_{2000}-RVG29 and (ii) DSPE-PEG_{2000}-TPP. (C) Expression of macrophage surface markers in extracted macrophages and formulations. (D) Morphological appearance of RVG/TPP-MASLNs-GS based on TEM. (E and F) Particle size (E) and zeta potential (F) distribution of nanoparticles (SLNs), biomimetic nanoparticles (MASLNs) without modification or modified with RVG29 (RVG-MASLNs) or TPP (TPP-MASLNs) alone, or with both RVG29 and TPP (RVG/TPP-MASLNs). (G) Size stability of bare SLNs, MASLNs and RVG/TPP-MASLNs in (i) PBS and in (ii) PBS with 10% FBS. (H) *In vitro* GS release from MASLNs or RVG/TPP-MASLNs in PBS (pH 7.4 or 6.0) at 37 °C.

was lyophilized and stored at −20 °C. Finally, DSPE-PEG_{2000}-TPP and DSPE-PEG_{2000}-RVG29 were respectively analyzed by MALDI-TOF mass spectrometry (MALDI-TOF MS) and H^1-NMR.

2.4. Macrophage membrane derivation

Fresh mouse peritoneal macrophages from c57BL/6J were harvested according to previously reported method with modification [25]. The mouse was intraperitoneal injected with 1 mL 3% thioglycolate broth for 3 days before sacrificed and disinfected by immersing in 75% ethanol. The body was then injected with 5 mL PBS containing 3% FBS in enterocoelia followed by full massage. The withdrawn PBS solution containing fresh peritoneal macrophage was spun at 1,500 RPM for 8 min. Cells were re-suspend in DMEM containing 10% FBS and were maintained in CO_2 incubator. The harvested macrophage ghost was prepared by 3 cycle of freezing and thawing in liquid nitrogen of macrophage suspension in 0.25× PBS with 50 nM PMSF. The lysate was washed with the buffer and centrifuged at 8,000 RPM to collect macrophage ghost.

2.5. Preparation of SLNs

SLNs were prepared by the solvent injection method with modification [26]. In brief, 60 mg of glycerol monostearate (GMS) and 4 mg GS were mixed in 1.0 mL of ethanol to form the oil phase and heated to 50 °C. Emulsifiers (containing 40 mg soya lecithin and 2% Tween 80) were dispersed in 10 mL distilled water with magnetic stirring at the same temperature. The heated oil phase was injected into the water phase by drop-by-drop followed by magnetic stirring for 30 min under 40 °C. After that, the O/W emulsion was poured into 10 mL of ice-cold water (~4 °C) and stirred continuously (1,000 RPM) under 4 °C for 30 min. Afterward, the organic solvent was removed from the system under reduced pressure by a rotatory evaporator (Rotavapor R-210, Buchi, Uster, Switzerland). Finally, SLNs-GS were appropriately condensed to reach a GS concentration of 0.5 mg/mL.

The GS encapsulation efficiency (EE) of the formulation was determined by minicolumn centrifugation using HPLC to quantify the GS in the SLNs [33]. The equation for the encapsulation efficiency is as follow:

$$EE\% = (W_{total\ GS} - W_{free\ GS}) / W_{total\ GS} \times 100\%.$$

2.6. Preparation of the biomimetic nanosystems

MA membranes were sonicated for 6 min using a bath sonicator (KQ3200; Kunshan, China) at a frequency of 37 kHz and a power of 100 W. Next, the resulting MA membrane vesicles were extruded repeatedly through 400-, 200-, and 100-nm polycarbonate porous membranes using a mini extruder (Avanti Polar Lipids, AL, USA).

To prepare plain MASLNs (MASLNs without a targeting ligand), 1 mL of GS-loaded SLNs or hydrophobic probe-tagged NPs at 5 mg/mL were mixed with 1 mL of MA membrane vesicles, followed by extrusion through a 100-nm polycarbonate membrane at least 5 times to obtain MASLNs-GS or hydrophobic probe-tagged MASLNs. Additionally, MASLNs with RVG29 modification (RVG-MASLNs), MASLNs with TPP modification (TPP-MASLNs) and those with both RVG29 and TPP modifications (RVG/TPP-MASLNs) were formed by the postinsertion method. Briefly, a lipid film of DSPE-PEG_{2000}-RVG29 (7.5%, molar ratio of DSPE-PEG_{2000}-RVG29 to SLNs) or DSPE-PEG_{2000}-TPP (5%, molar ratio of DSPE-PEG_{2000}-RVG29 to SLNs) was prepared by rotary evaporation and was further dried under vacuum for 24 h. The dried lipid film was subsequently hydrated with PBS (pH 7.4) to the formation of micelles at 37 °C. For the RVG-MASLNs or TPP-MASLNs preparations, a micelle solution of DSPE-PEG_{2000}-RVG29 or DSPE-PEG_{2000}-TPP was added into preformed MASLNs and was incubated for 4 h at 37 °C in PBS (pH 7.4), respectively.

2.7. Characterization of the biomimetic nanosystems

Nanoparticle size (diameter, nm) and surface charge (zeta potential, mV) of the prepared formulations were measured by dynamic light scattering (DLS) (Litesizer 500, Anton Parr, Austria). The morphology of RVG/TPP-MASLNs was characterized via transmission electron microscopy (TEM) (HITACHI, H-7650, Japan). Prepared formulations in 1× PBS or PBS containing 10% FBS were kept in 37 °C for the analysis of stability by measurement of particle diameter within 60 h.

2.8. In vitro release profile

Dialysis bags (MW. Cutoff: 14 kDa) with 1 mL of GS-loaded formulations were directly immersed into 30 mL of PBS (0.1 M, pH 7.4) or PBS (0.1 M, pH 6.0). At preset time points, 800 μL aliquots were withdrawn from the solution and the same volume of PBS was added. The GS in the obtained samples was measured using HPLC as mentioned above.

2.9. Western blot

Western blot analysis was performed as described previously [34]. Briefly, the collected samples of NPs, cell pellets or brain tissues were lysed in cold T-PER buffer containing 1% phosphatase inhibitors and complete mini cocktail (Roche, Switzerland). Protein concentrations were measured by the Bicinchoninic (BCA) assay kit (Pierce, China). Twenty micrograms of each protein sample were resolved by sodium dodecyl sulfate-polyacrylamide gel electrophoresis (SDS-PAGE). Gels were then transferred to polyvinylidene difluoride (PVDF) membranes (Millipore Corporation, USA). Transblotted PVDF membranes were blocked with 5% BSA for 1 h and then incubated overnight with the indicated primary antibody in 1% BSA at 4 °C and followed by the secondary antibody conjugated with horseradish peroxidase. Blots were visualized using ECL-Plus according to the manufacturer's instructions.

2.10. Cytotoxicity of empty biomimetic nanosystems

HT22 were seeded and differentiated in 96-well plates at 37 °C in a 5% CO_2 atmosphere. bEnd.3 cells and astrocytes were seeded into 96-well plates and incubated at the same condition for 24 h. Then, the cells were treated with different empty formulations and were incubated for another 24 h. At the end of the incubation, cell viability was evaluated using MTT method.

2.11. In vivo safety evaluation

The healthy mice were randomly divided into six groups (n = 6) and were treated with saline (control), free GS solution, various GS-loaded formulations at a single GS dose of 5 mg/kg body weight via the tail vein, respectively. The daily body weight was recorded every day. At day 14, these mice were sacrificed, and samples of the heart, liver, spleen, lung, kidney and brain were treated as mentioned above and sectioned at 8 μm thickness. The sections were then mounted on slides and stained with hematoxylin and eosin (H&E).

2.12. Antiphagocytosis ability of the biomimetic nanosystems

Mouse peritoneal macrophages were seeded into a Petri dish in DMEM with 10% FBS at 37 °C in a 5% CO_2 atmosphere. 4 h later, cells were washed to remove non-adherent cells and the culture mediem was renewed. After 24 h, the cells were incubated with 5 μM Cou6-tagged NPs (SLNs-Cou6, MASLNs-Cou6 and RVG/TPP-MASLNs-Cou6) for 4 h. After incubation, the cells were collected and analyzed via flow cytometry (FCM) (BD FACSCalibur, USA).

2.13. Pharmacokinetic studies

SD rats (190–210 g) were fasted overnight prior to administration but allowed free access to water. Rats were randomly divided into four groups (n = 6). The pharmacokinetic profiles of GS-loaded biomimetic nanosystems were measured with a single dose of 5 mg/kg GS by tail vein injection. Additionally, free GS soluted in a co-solvent of water/alcohol was injected into the other group of rats for pharmacokinetic comparison, as reported in previous studies [33]. Blood was sampled from the retro-orbital sinus at different time points. Rat plasma (50 μL) was diluted in methanol 1:1 with acentonitrile containing internal standard (IS) (150 ng/ml chrysine). The sample was vortexed, followed by centrifugation at 8,000× g for 5 min. The upper layer was removed and analyzed for GS via liquid chromatography-tandem mass spectrometry (LC-MS/MS) as described previously [35]. Briefly, analysis of GS and the IS was performed on PE Series 200 HPLC system coupled online to a PE Sciex API 3000 triple quadrupole mass spectrometer with an ESI interface, using a Discovery HS C18 column (5 cm× 2.1 mm; 3 μm). The mobile phase was composed of (A) 5 mM ammonium acetate (pH = 7.0) and (B) acetonitrile with a gradient of 5–95% B eluted over

11 min at a flow rate of 200 μL/min. Quantification was achieved by electrospray ionization (ESI) mass spectrometer in negative ion mode utilizing Multiple Reaction Monitoring (MRM). Data were obtained and analyzed by Analyst 1.6 software. DAS 2.0 software was used to model the data of the experiment.

2.14. Cellular uptake and colocalization into the mitochondria

HT22 cells were seeded into a Petri dish and differentiated as mentioned above. Astrocytes were seeded at the same condition as HT22 cells. HT22 cells or astrocytes were incubated with 5 μM Cou6-tagged formulations for 4 h. Live cells were harvested and resuspended in PBS for cellular uptake analysis via flow cytometry (FCM) (BD FACSCalibur, USA). For mitochondrial colocalization analysis, the Cou6-tagged formulations-treated cells (5 μM, 4 h) were then stained with 0.5 μM MitoTracker Red (Molecular Probes, USA), followed by washing and keeping in pre-warmed PBS. Finally, cells were analyzed by confocal laser scanning microscopy (CLSM) (UltraVIEW Vox, PerkinElmer, USA) as soon as possible. The Pearson's co-localization coefficient was processed and calculated by Image J software.

2.15. Transport across BBB and targeting of neuron cells

BBB-astrocytes and BBB-HT22 cells model were respectively established according to previous reports [36], with minor modifications. Briefly, bEnd.3 cells were seeded onto the upper chamber of the Transwell (Corning, NY, USA) and astrocytes were seeded in the bottom chamber at 37 °C and 5% CO_2. After the co-culture of bEnd.3 cells (upper chamber) and astrocytes (bottom chamber) for 11 days, a tight monolayer (transendothelial electrical resistance (TEER) reached 308.9 ± 4.3 Ω cm^{-2}) was formed for BBB-astrocytes model. BBB-HT22 model was established on the basis of BBB-astrocytes model. Briefly, after the establishment of BBB-astrocytes model, the upper chamber with the bEnd.3 monolayer was transfer to another bottom chamber seeded with differentiated HT22 cells. The regrouped bEnd.3 monolayer (upper chamber) and HT22 cells (bottom chamber) were then co-cultured for another 1 day (TEER reached 313.6 ± 3.7 Ω cm^{-2}) to form the BBB-HT22 model. Then different 5 μM Cou6-tagged formulations were added to the apical compartment. After incubation for 12 h, fluorescent signals of the HT22 cells or astrocytes in the lower chamber were observed via FCM.

2.16. In vivo imaging

Near-infrared dye DIR was applied as the fluorescence probe to evaluate the brain targeting efficiency of biomimetic nanosystems to mice. These mice were administered different DIR-tagged formulations via tail vein injection. 1 h after i.v. injection, *in vivo* imaging was performed using IVIS Lumina II (Caliper Life Science, USA). After the image collection, the liver and spleen were rapidly harvested for *ex vivo* imaging. Meanwhile, the brain was separated, washed with saline, blotted with filter paper, weighed and homogenized (tissue: saline = 1: 3, w/w). The fluorescent signal of DIR in brain homogenate was measured by Tecan Spark microplate reader (Tecan (Shanghai) Trading Co., Ltd) at Ex/Em = 748/780 nm.

2.17. Mitochondrial and intracellular ROS measurement

Differentiated HT22 cells were cultured in 6-well plates. Cells were treated with different GS-loaded formulations for 4 h and then co-cultured with $A\beta_{25\text{-}35}$ (at a final concentration of 30 μM) for another 20 h. The final concentration of each GS was 5 μg/mL. The relative levels of mitochondrial ($\cdot O_2^-$ in mitochondria) and intracellular (H_2O_2) ROS were respectively measured using MitoSOX (Molecular Probes, USA) and CM-H_2DCFDA (Molecular Probes, USA) as fluorescent probes via flow cytometry (FCM) (BD FACSCalibur, USA).

2.18. Cell apoptosis assay

Differentiated HT22 cells were treated with GS-loaded formulations and co-cultured with $A\beta_{25\text{-}35}$ as the method described above. Following 24 h of incubation, the cells were collected and stained using the Annexin V-FITC/PI apoptosis detection kit (Solarbio Science & Technology Co., Ltd, Beijing, China) according to the manufacturer's instructions and were immediately analyzed by FCM.

2.19. Morris water maze (MWM) behavioral test

The 9-month-old APP/PS1 mice were randomly divided into five groups (20 mice in each group) and were treated with saline (control), free GS solution and various biomimetic nanosystems carrying GS by i.v. injection every two days for a total of 30 d at a concentration of 2 mg/kg of GS. Next, after the last administration, the mice were trained and tested in the Morris water maze (MWM) as described previously [37]. Briefly, the mice were trained three times a day for 5 days. Finally, on the sixth day, with the platform removed, the mice were placed into the tank from the same fixed positions and were allowed to swim freely for 90 s with the times of platform crossing recorded. The mouse trajectory and escape latency were recorded using a computer-controlled tracking system (Shanghai Jiliang Software Technology Co., Ltd.).

2.20. Histological examination

To evaluate morphological features of the neurons in the dentate gyrus of the hippocampus, brains of mice were collected and fixed in 10% formalin, embedded in paraffin, and sectioned at 8 μm thickness. The sections were then mounted on slides and stained with H&E, and observed and photographed under an optical microscope.

2.21. Enzyme-linked immunosorbent assay (ELISA) for IL-6 and TNF-α measurements in brain

After MWM behavioral test, APP/PS1 mice were sacrificed. Brain tissues were lysed in buffer containing 50 mM Tris (pH 7.4), 150 mM NaCl, 1% Triton X-100, 1% sodium deoxycholate, 0.1% SDS and protease inhibitors. The homogenate was sonicated and centrifuged (12,000 RPM, 20 min, 4 °C), and the supernatant was kept for further analysis. Collected samples were respectively measured via Mouse IL-6 ELISA Kit and Mouse TNF-α ELISA Kit (Beyotime Biotechnology Co., Ltd., China) according to the manufacturer's instructions.

2.22. Oxidative stress-related biomarker assay in the hippocampus

After MWM behavioral test, APP/PS1 mice were sacrificed. The brain hippocampus tissues were collected and lysed in buffer as mentioned above. SOD activities and MDA levels in hippocampal area were respectively measured via Total Superoxide Dismutase Assay Kit and Lipid Peroxidation MDA Assay Kit (Beyotime Biotechnology Co., Ltd., China) according to the manufacturer's instructions.

2.23. Inflammation-related astrocytes and microglia activation in hippocampus

After MWM behavioral test, APP/PS1 mice were sacrificed. The brain hippocampus tissues were collected and lysed in buffer as mentioned above. GFAP and Iba-1 levels were measured via western blotting method as mentioned above.

2.24. Statistical analysis

All data are presented as the means ± standard deviation (SD). The data were analyzed using one-way ANOVA coupled with Dunnett post

hoc analysis to carry out multigroup comparison. Comparison between two groups was accomplished via an unpaired two-tailed student's t-test. $p < 0.05$ indicated a statistically significant difference.

3. Results and discussion

3.1. Preparation and characterization of nanocarriers

The preparation scheme for RVG/TPP-MASLNs-GS is illustrated in Fig. 1A. First, the MA membranes with high expression of F4/80 and CD11b ("outer shell" of the biomimetic nanosystems) were derived from mouse peritoneal macrophage, and solid lipid nanoparticles (SLNs) ("inner core" of the biomimetic nanosystems) were prepared using solvent injection method. Next, the resulting MA membranes were coated onto the surface of SLNs through mechanical extrusion to form MA membrane-coated solid lipid nanoparticles (MASLNs) with a characteristic core-shell structure (Fig. 1D). To improve targeting efficiency, the MASLNs were modified using two synthesized functional conjugates, DSPE-PEG_{2000}-RVG29 and DSPE-PEG_{2000}-TPP. We conjugated amino-RVG29 to the distal end of DSPE-PEG_{2000}-MAL by the reaction of thiol with the active group MAL (Fig. 1B). Similarly, DSPE-PEG_{2000}-TPP was synthesized by the reaction of carboxyl groups on TPP with the active group NH_2 contained in DSPE-PEG_{2000}-NH_2 (Fig. 1B). The purified materials were obtained by dialysis (MWCO 3.5 kDa) against distilled water. Successful synthesis was evidenced by the band coincidence in H^1-NMR (Fig. S1B) and the molecular shifts in MALDI-TOF MS analysis (Fig. S1A).

Macrophages were disrupted by repeated freezing and thawing, and centrifuged to isolate the MA membranes. F4/80 and CD11b are two macrophage markers expressed on cell membranes. In order to confirm whether the nanosystems camouflaged by MA membranes possess the biological mark of general macrophages, the expression of both F4/80 and CD11b were detected by Western blot measurements compared with macrophages and purified MA membranes (Fig. 1C). Na,K-ATPase and β-actin signals in these samples were measured as a control. The specific protein signals of F4/80 and CD11b were obviously observed in macrophages, MA membrane and MA membrane-camouflaged nanosystems, which validated the presence of these markers (Fig. 1C). Na,K-ATPase, as the internal reference of membrane protein, showed a similar expression level in each sample (Fig. 1C). In addition, the β-actin signals were readily detected in macrophages but were barely observed in purified MA membrane, MASLNs nor RVG/TPP-MASLNs, which denoted the high purity of the isolated MA membrane and no interference of cell actins on the decoration in MA membrane-camouflaged nanosystems (Fig. 1C).

For nanoparticles, the particle size and zeta-potential are crucial factors that determine the fate of nanoparticles. All five formulations showed an even distribution in size less than 140 nm (Fig. 1E and Table S1). This particle size was suitable for the particles in blood to cross into the tissue, approach cell surface receptors and facilitate intracellular transport [38]. As shown in Fig. 1D, the TEM images of RVG/TPP-MASLNs demonstrated that the particle sizes were close to those measured using the laser particle analyzer. The zeta potentials of ligand-modified biomimetic nanosystems (TPP-MASLNs and RVG/TPP-MASLNs) were higher than that of MASLNs (Fig. 1F and Table S1), owing to the positive charge of the TPP. This would be beneficial for the internalization of ligand-modified biomimetic nanosystems, because the cell membranes and mitochondrial membranes are negatively charged. Because stability is a prerequisite for further applications *in vivo*, the agglomerations of the biomimetic nanosystems in PBS and PBS with 10% FBS were respectively evaluated within 60 h at 37 °C to mimic *in vivo* conditions. The results indicated that both MASLNs and RVG/TPP-MASLNs exhibited good stability while bare SLNs aggregated after storage in PBS containing 10% FBS.

The *in vitro* GS release study at different pH conditions was also performed to examine the drug release property of the GS-loaded biomimetic nanosystems. As shown in Fig. 1H, both MASLNs-GS and RVG/TPP-MASLNs-GS demonstrated sustained release behaviors with no initial release burst at normal physiological pH. Evidences shows that the spherical nanoparticles internalized into cells need to overcome the acid endosome (pH ranges from 5.5 to 6.5) barrier to enter the cytoplasm [50]. Thus, the prerequisite for RVG/TPP-MASLNs-GS to target the neuronal mitochondria is that the delivery system remains stable in the acidic environment of endosome. According to the results, both MASLNs-GS and RVG/TPP-MASLNs-GS maintained a sustained release behaviors at pH 6.0, indicating the relative stability in endosome with the acidic pH. Similar release patterns between MASLNs-GS and RVG/TPP-MASLNs-GS at every time point implied that ligand modifications didn't significantly affect the release behavior. Similar physicochemical characteristics of these formulations allowed us to specifically compare the effects of ligand modification on the anti-AD abilities of the biomimetic nanosystems.

3.2. Preliminary safety test

In addition to having suitable physiochemical properties, an ideal nanocarrier should have minimal toxicity and high biocompatibility. We first conducted MTT assays of the various empty biomimetic nanosystems to assess their safety *in vitro*. As shown in Fig. 2A–2C, the viabilities in the differentiated HT22 neurons (Fig. 2A), bEnd.3 cells (Fig. 2B) or astrocytes (Fig. 2C) of each group were higher than 90% after incubation with the detected doses of the empty biomimetic nanosystems for 24 h, revealing that these biomimetic nanosystems were relatively safe.

For *in vivo* safety assessment, no obvious abnormal state was observed among the tested mice within 14 days. Furthermore, on day 14, tissue sections from the heart, liver, spleen, lung, kidney and brain were assayed via H&E staining after intravenous administration using different samples in healthy mice. As shown in Fig. 2D, compared with the saline (control) group, no indicators of damage were observed for these organs after treatment, suggesting that GS solution and MASLNs-GS did not cause systemic toxicity by i.v. injection at the current GS dosage. Similar results were found in RVG/TPP-MASLNs-GS group, suggesting that ligand modifications did not significantly affect the biocompatibility of the biomimetic nanosystems. Taken together, these results confirmed the low toxicity and good biocompatibility of RVG/TPP-MASLNs-GS, possibly due to biodegradation of the "inner core" and endogenous property of the "outer shell".

3.3. Reticuloendothelial system (RES) evasion features

The reticuloendothelial system (RES) evasion ability of nanosystems is crucial to extand the residential time during systemic circulation to achieve targeting delivery. To verify whether RVG/TPP-MASLNs-GS inherit the immunological characteristics of macrophages, the *in vitro* antiphagocytosis assay was first conducted. Mouse peritoneal macrophages were utilized as a cell model to reckon the stealth power of the biomimetic nanosystems. A less fluorescence level was visualized in macrophages treated with MASLNs-Cou6 and RVG/TPP-MASLNs-Cou6 than in the bare SLNs-Cou6 group (Fig. 3A), indicating that the MA membrane coating may effectively block nonspecific phagocytose by macrophages. Meanwhile, MA membrane-coated SLNs (MASLNs and RVG/TPP-MASLNs) were less trapped by liver and spleen (Fig. S2). The results implied that MA membranes could camouflage these bare SLNs from being eliminated by RES-rich organs in circulation.

After a series of *in vitro* studies, a pharmacokinetics study was employed to investigate the *in vivo* behavior of GS-loaded formulations (Fig. 3B and Table S2). It was found that both MASLNs-GS and RVG/TPP-MASLNs-GS showed initially high blood circulating levels, while bare SLNs-GS and free GS solution were more quickly cleared from the systemic circulation. The results confirmed the RES evasion feature of biomimetic nanosystems *in vivo*, possibly due to the self identification

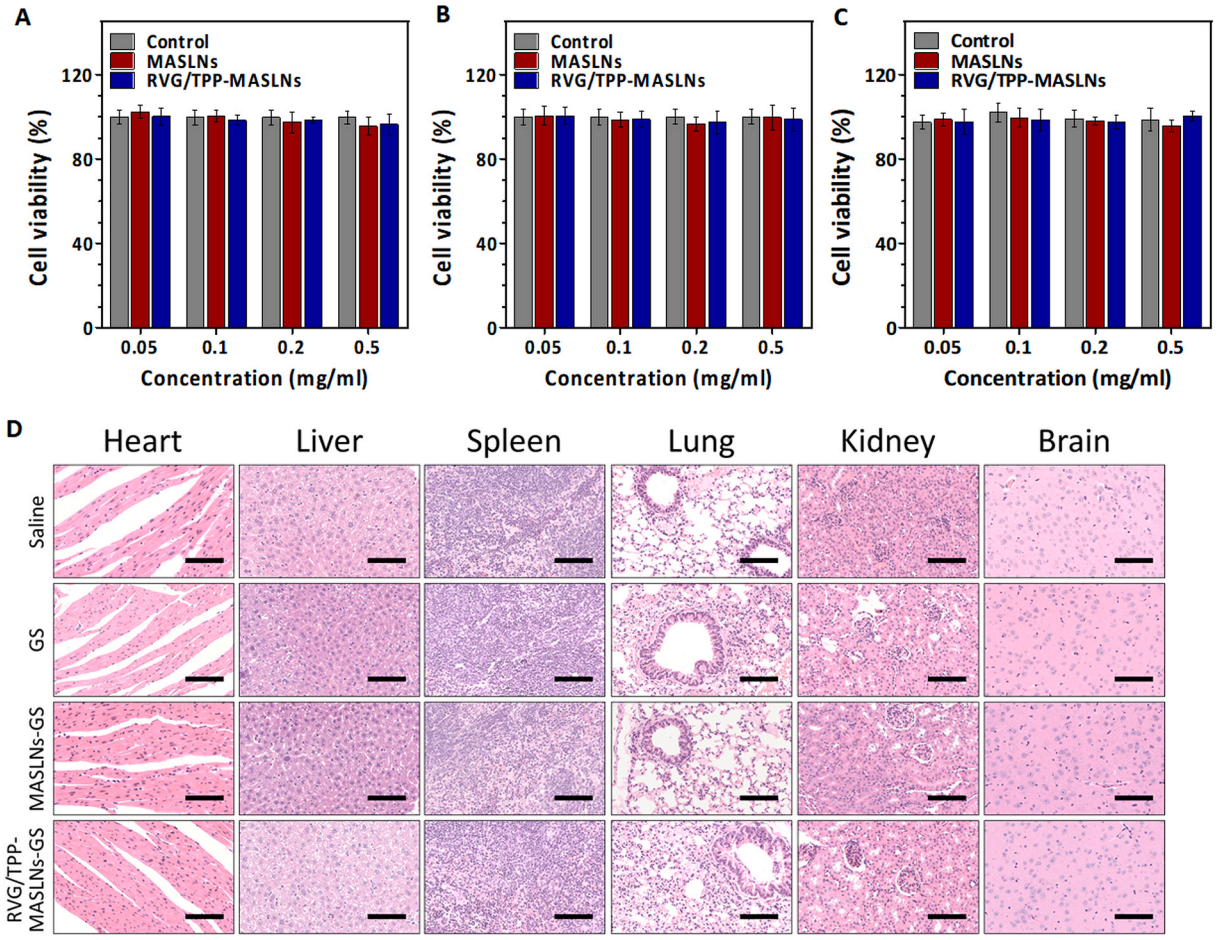

Fig. 2. Preliminary safety evaluation of the biomimetic nanosystems. (A–C) Cell viability of HT22 (A) cells, bEnd.3 (B) cells and astrocytes (C) incubated for 24 h with different concentrations of empty formulations. The data are presented as the means ± SD (n = 6). (D) Histological staining of organs from healthy mice treated with different GS-loaded formulations (scale bar = 100 μm).

property of the "outer shell" to macrophages (Fig. 3A), as well as the sustained drug release profile (Fig. 1H) of the "inner core". Additionally, MASLNs-GS and RVG/TPP-MASLNs-GS displayed resembling pharmacokinetic curves, and no significant difference was observed in the AUC, $t_{1/2\alpha}$, $t_{1/2\beta}$, MRT and CLz between them ($p > 0.05$) (Table S2). Thus, the post-insertion of RVG29 and/or TPP onto the surface of the biomimetic nanosystems did not impair the RES evasion characteristic of MA membranes. The results again emphasized the advantage of the postinsertion method in preparing ligand-modified biomimetic nanosystems.

3.4. Neural mitochondria-targeting and transport across the BBB of the biomimetic nanosystems

To assess the potential neuronal mitochondria targeting capability of ligand-modified biomimetic nanosystems, the neuronal cellular uptake of various Cou6-tagged formulations was conducted. As shown in Fig. 4A, the ligand-modified formulations (TPP-MASLNs-Cou6, RVG-MASLNs-Cou6 and RVG/TPP-MASLNs-Cou6) were significantly internalized into differentiated HT22 neurons compared with non-modified formulations (MASLNs-Cou6), indicating that ligands could sufficiently improve entrance into the cells. Among all the tested formulations, RVG/TPP-MASLNs-Cou6 exhibited the maximum intracellular

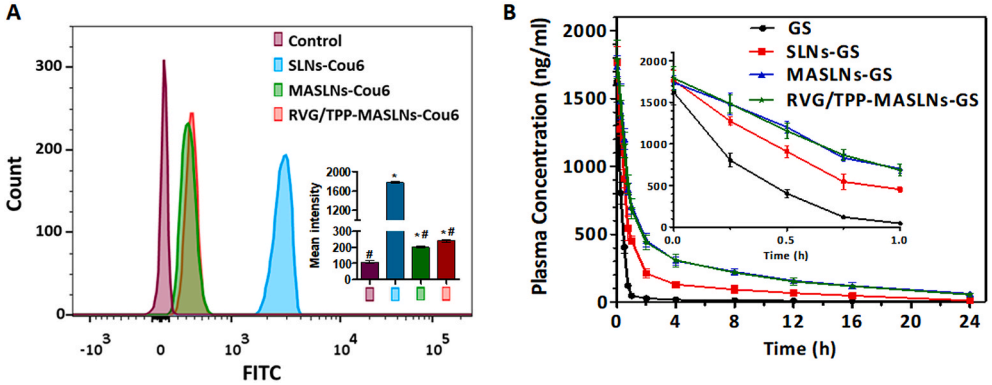

Fig. 3. RES evasion features of RVG/TPP-MASLNs. (A) FCM analysis of mouse peritoneal macrophages after incubation with various Cou6-tagged formulations. $^{*}p < 0.05$ compared with the Control group. $^{\#}p < 0.05$ compared with the SLNs-Cou6 group. (B) Plasma GS concentration-time profiles after i.v. injection of different formulations in rat. The data are presented as the means ± SD (n = 6).

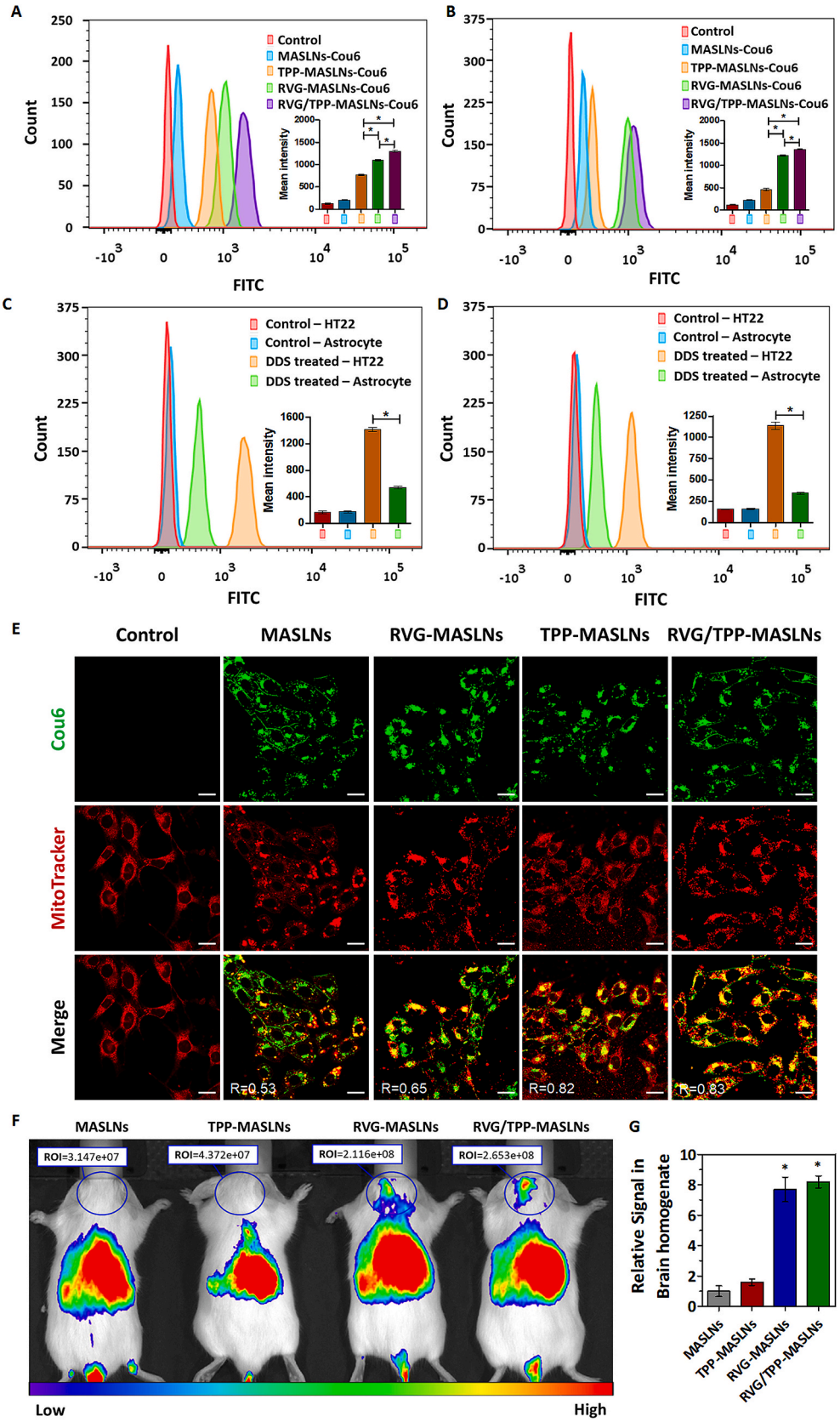

Fig. 4. Neural mitochondria-targeting and transport across the BBB of the biomimetic nanosystems *in vitro* and *in vivo*. (A) Neuronal cellular uptake via FCM analysis of differentiated HT22 cells after incubation with different Cou6-tagged formulations. (B) FCM analysis of differentiated HT22 cells treated with various Cou6-tagged formulations after crossing the bEnd.3-HT22 cells co-culture BBB model *in vitro*. (C) Comparison of the selective targeting ability of the DDS (RVG/TPP-MASLNs-Cou6) between HT22 neurons and astrocytes. (D) Comparison of the remaining ability of the DDS (RVG/TPP-MASLNs-Cou6) for selective targeting after crossing the bEnd.3-HT22 cells or bEnd.3-astrocytes co-culture BBB model *in vitro* by FCM. * indicates $p < 0.05$. (E) Colocalization of various Cou6-tagged formulations into mitochondria in differentiated HT22 cells. Cou6 (green) and MitoTracker for mitochondria staining (red) were recorded. Scale bars represent 20 μm. R represents the co-localization coefficient determined using Image J software. (F) *In vivo* brain-targeting ability. Biodistribution of DIR contained in various formulations determined by IVIS Lumina II. (G) Relative fluorescence signal of brain homogenate after *in vivo* image acquisition. Data are presented as means ± SD (n = 3). *$p < 0.05$ compared with MASLNs.

fluorescence intensity due to dual-mediated endocytosis. The specific binding of RVG29 to nAChR expressed on neurons is speculated as the main reason for the increased uptake of ligand-modified carriers by neurons [39,40], for the strongest fluorescence intensity of RVG-MASLNs-Cou6 and RVG/TPP-MASLNs-Cou6) were detected in neurons (Fig. 4A). Additionally, anchoring TPP on the biomimetic nanosystems changes the nanosystem's surface charge (Fig. 1F and Table S1), enhancing its cell association and entrance into the cells by membrane

partitioning [41].

One of the challenges in the treatment of ROS-induced mitochondrial dysfunction is the lack of carriers for delivering antioxidants into neuronal mitochondria. To explore whether these ligand-modified formulations targeted the mitochondria after successful internalization into neurons, mitochondrial colocalization study was conducted. Fig. 4E illustrates images for the colocalization of the biomimetic nanosystems into the mitochondria of differentiated HT22 cells after treatment with various Cou6-tagged formulations. Bright-yellow fluorescence by red (mitochondria) merging with green (Cou6-tagged formulations) fluorescence was used to indicate the colocalization of the Cou6-tagged biomimetic nanosystems into the mitochondria. According to Fig. 4E, RVG/TPP-MASLNs evidently localized in the mitochondria of HT22 cells (co-localization coefficient R was 0.83). Although RVG-MASLNs can easily internalize into HT22 cells (Fig. 4A and E), the mitochondrial colocalization (R = 0.65) in HT22 cells were not ideal compared with RVG/TPP-MASLNs (R = 0.83). The results indicated that RVG29 could not recognize and bind to the mitochondria. Thus, RVG-MASLNs could not effectively target mitochondria. Meanwhile, a comparable degree of colocalization of fluorescence with the mitochondrial compartment was found for TPP solely-functionalized formulations (TPP-MASLNs (R = 0.82) compared with that for RVG/TPP-MASLNs (R = 0.83). It is reported that TPP could drive the modified nanoparticles to translocate to mitochondria [51]. Thus, based on these results, we conclude that RVG29 and TPP are responsible for different segments during the delivery process of RVG/TPP-MASLNs. Among them, the neuronal mitochondria-targeting ability of the biomimetic nanosystems after internalization into neurons was mainly potentiated by the TPP instead of RVG29.

The ability to cross the BBB is one of the major prerequisites for nanocarriers to mediate neuronal mitochondria-targeting drug delivery. After the neuronal mitochondria-targeting ability of TPP-modified formulations was verified, BBB permeability studies were conducted via a bEnd.3/HT22 co-culture BBB model *in vitro*. As shown in Fig. 4B, the fluorescence intensity remains a very low level in the lower chamber of HT22 cells after incubating with MASLNs-Cou6 for 12 h, indicating that it could not effectively pass through the BBB. The difference in the cellular uptake in the co-culture model between MASLNs-Cou6 and TPP-MASLNs-Cou6 was not remarkble, implying TPP's lack of adequate BBB permeability, whereas the relative high uptake in TPP-MASLNs-Cou6-treated HT22 cells was derived from the promoted entry of nanosystems into cells via TPP (Fig. 4A). By contrast, a significant signal was observed in the bottom chamber of HT22 cells with the treatment of both RVG-MASLNs-Cou6 and RVG/TPP-MASLNs-Cou6, suggesting that the RVG29-modified formulations could pass through the BBB and internalize into HT22 cells. Among all the groups, RVG/TPP-MASLNs-Cou6 held the most efficient permeability of BBB, indicating that the dual-modified formulations could efficiently cross the BBB and sufficiently promote uptake in HT22 cells under the synergistic effect of RVG29 and TPP.

However, glial cells are generously existed in the central nervous system in addition to neurons. The selective targeting of the drug delivery system (DDS) to neurons is another key direction after it enters the central nervous system. The specific targeting ability of the RVG29-modified DDS to neurons was evaluated via comparing the internalizations of the DDS by differentiated HT22 neurons and astrocytes. As shown in Fig. 4C, the fluorescence intensity in DDS treated-HT22 neurons was significantly higher than that in DDS treated- astrocytes, indicating a relative higher selectivity of the DDS to neurons than to astrocytes. The remaining ability of the DDS for selective targeting to neurons after crossing the BBB was further verified via the bEnd.3/HT22 or bEnd.3/astrocytes co-culture BBB models (Fig. 4D). By contrast, the internalization of the DDS in HT22 neurons was still significantly higher than that in astrocytes after crossing the BBB, suggesting the selectively targeting priority of the DDS to neurons in the central nervous system. Taken together, the results again emphasize the advantage of RVG29, which can efficiently cross the BBB into neuron cells with higher selectivity [27,28].

To verify the actual penetrating BBB ability of RVG/TPP-MASLNs, *in vivo* imaging was performed on mice using various DIR-tagged biomimetic formulations by tail vein injection. Based on whole-body imaging (Fig. 4F), the brain accumulation of DIR-tagged MASLNs and TPP-MASLNs did not occur evidently. By contrast, high accumulation of DIR-tagged RVG-MASLNs was detected in the brain at 1 h after injection. Importantly, the most intense distribution in the brain was displayed in the DIR-tagged RVG/TPP-MASLNs-treated mice and was further confirmed by the fluorescence intensity identified in the isolated brain homogenate (Fig. 4G). This phenomenon indicated that the introduction of RVG29 induced brain targeting of the nanosystem, and the incorporation of TPP further enhancing its accumulation in neurons. The *in vivo* imaging results agreed with the results of the *in vitro* co-culture model shown in Fig. 4B. These initial data demonstrated that RVG29-functionalized formulations (RVG-MASLNs and RVG/TPP-MASLNs) could pass through the BBB efficiently. Overall, these above results (Fig. 4) demonstrated that the dual-modified biomimetic nanosystems could not only penetrate BBB but also target the neuron cells and further localize in the mitochondria under the synergistic effect of RVG29 and TPP.

3.5. *In vitro* antioxidative stress effect

The protection of mitochondria against oxidative stress from ROS is therapeutically beneficial to AD [42]. The protective role of genistein in neuron cells, along with the potent antioxidant and free radical scavenging activity, has been widely studied [12,43]. Accordingly, we studied the mitochondria as a therapeutic target against AD and evaluated the *in vitro* antioxidative stress effects using GS-loaded biomimetic nanosystems. The scavenging capacity of GS-loaded formulations for mitochondrial ROS ($\cdot O_2^-$) was measured by FCM (Fig. 5A). We found that $A\beta_{25\text{-}35}$ induced the upregulation of the mitochondrial ROS level, that is consistent with the previous studies [44]. Interestingly, TPP-functionalized formulations (TPP-MASLNs-GS and RVG/TPP-MASLNs-GS) could more strongly inhibit mitochondrial ROS in Aβ-treated HT22 neuronal cells after targeting mitochondria than other groups, a finding that could be attributed to TPP-mediated delivery. As we expected, RVG/TPP-MASLNs-GS presented the strongest inhibition of mitochondrial ROS. By contrast, the inhibitory capability of RVG-MASLNs-GS and MASLNs-GS was not ideal, likely attributed to their lack of mitochondria-targeting ability. These results were consistent with the mitochondrial colocalization (Fig. 4E) described above.

Intracellular H_2O_2 is a toxic byproduct of aerobic metabolism, which is related to signal pathways and plays a crucial role in oxidative stress and cellular apoptosis. Intracellular H_2O_2 levels were measured to further determine whether these GS-loaded formulations reduced oxidative stress from ROS in the Aβ-treated HT22 neuronal cells (Fig. 5B). Although TPP-functionalized formulations are predominantly targeted to mitochondria, TPP-MASLNs-GS did not cause more powerful anti-oxidative stress than RVG-MASLNs-GS for the reason of the less internalization into HT22 neuronal cells (Fig. 4A). Compared with other groups, RVG/TPP-MASLNs-GS exhibited the greatest anti-oxidative stress effect in the Aβ-treated HT22 cells, a finding that was consistent with the data presented regarding cellular uptake (Fig. 4A) and mitochondria targeting (Fig. 4E).

Mitochondrial ROS accumulation is known to be a major cause of neuronal apoptosis, and ROS clearance can benefit the viability to rescue mitochondrial pathology [29]. Because TPP-functionalized formulations containing GS can inhibit mitochondrial ROS, we further evaluated whether they affected cell apoptosis. As shown in Fig. 5C, the apoptosis of HT22 cells was increased to 50.27% when the cells were stimulated with $A\beta_{25\text{-}35}$. Consistent with these findings in mitochondrial ROS measurement, RVG/TPP-MASLNs-GS treatment decreased the cell apoptosis rate to 14.35%, much more effective than TPP-

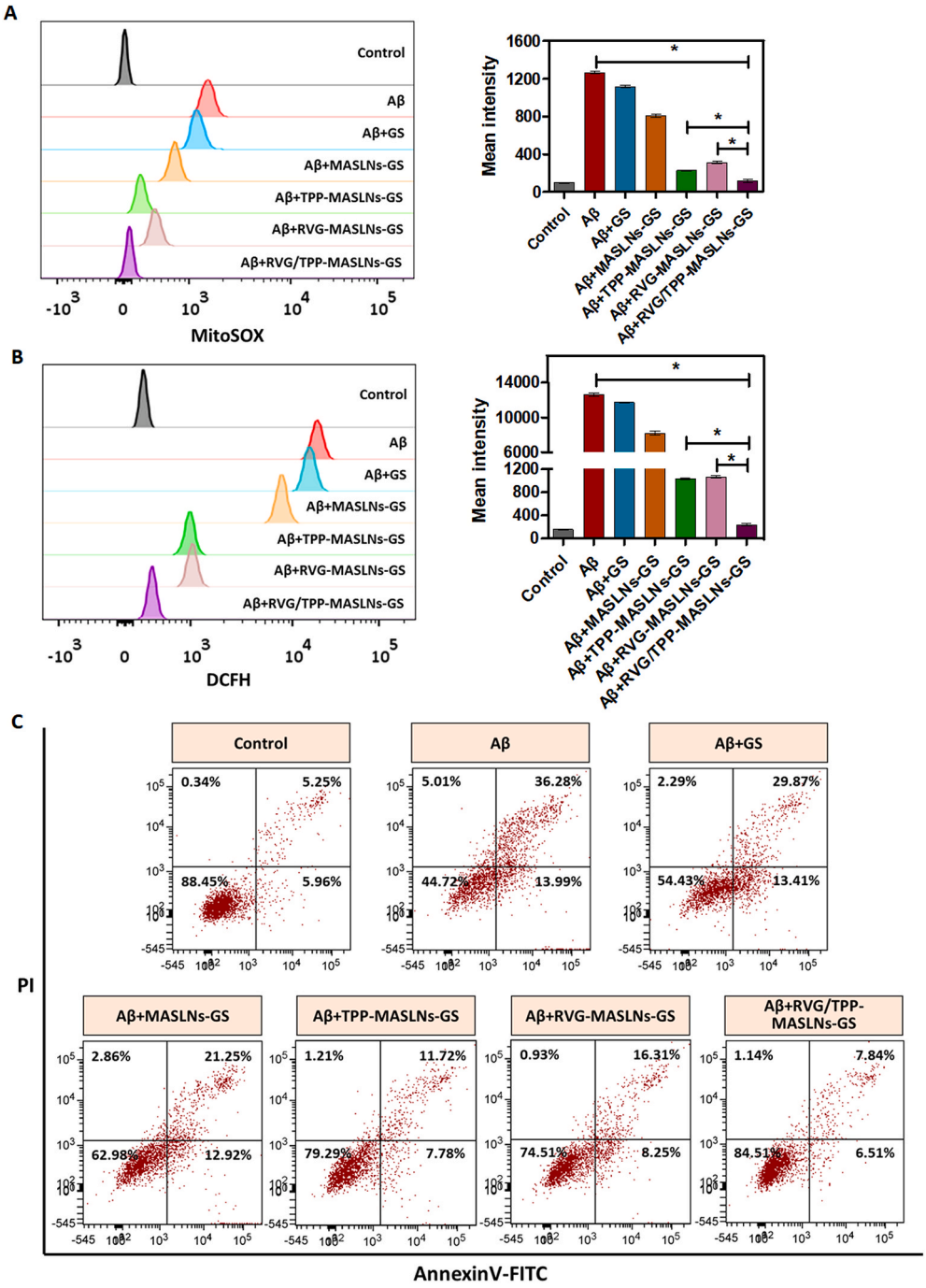

Fig. 5. Therapeutic effect of GS-loaded biomimetic nanosystems *in vitro*. (A and B) FCM analysis of mitochondrial ROS accumulation obtained by MitoSOX (A) and intracellular H_2O_2 level by CM-H_2DCFDA (B) in A$\beta_{23\text{-}35}$-damaged HT22 cells after treatment with different GS-loaded formulations. * indicates $p < 0.05$. (C) Anti-apoptosis results of A$\beta_{23\text{-}35}$-damaged HT22 cells after treatment with different GS-loaded formulations.

MASLNs-GS (19.50% apoptosis), RVG-MASLNs-GS (24.56% apoptosis), MASLNs-GS (34.17% apoptosis) and free GS treatment (43.28% apoptosis), respectively. The results demonstrated that RVG/TPP-MASLNs-GS can effectively protect HT22 neurons from apoptosis.

3.6. Reverse of the cognitive deficits in APP/PS1 transgenic mice by RVG/TPP-MASLNs-GS

With advantages in suitable physiochemical properties, the RES evasion features, safety, multi-targeting abilities and *in vitro* anti-oxidative stress effect, we subsequently evaluated the effect of RVG/TPP-MASLNs-GS in alleviating the progression of AD pathology. The MWM test was used to detect whether the GS-loaded dual-modified biomimetic nanosystems could improve spatial learning ability in APP/PS1 mice. As shown in Fig. 6A–6D, saline treatment APP/PS1 group showed significant learning deficits. Due to the weak BBB-penetrating efficiency, APP/PS1 mice treated with GS solution or TPP-MASLNs-GS showed slightly improved learning ability. Owing to the high BBB penetrating efficacy, APP/PS1 mice moderately alleviated defects following the administration of RVG-MASLNs-GS. Furthermore, RVG/TPP-MASLNs-GS significantly improved the cognitive ability of APP/PS1 mice by shortening the escape latency (Fig. 6A), increasing the frequency of across the platform (Fig. 6B), prolonging the time spent in a targeted quadrant after removing the platform (Fig. 6C), and restoring

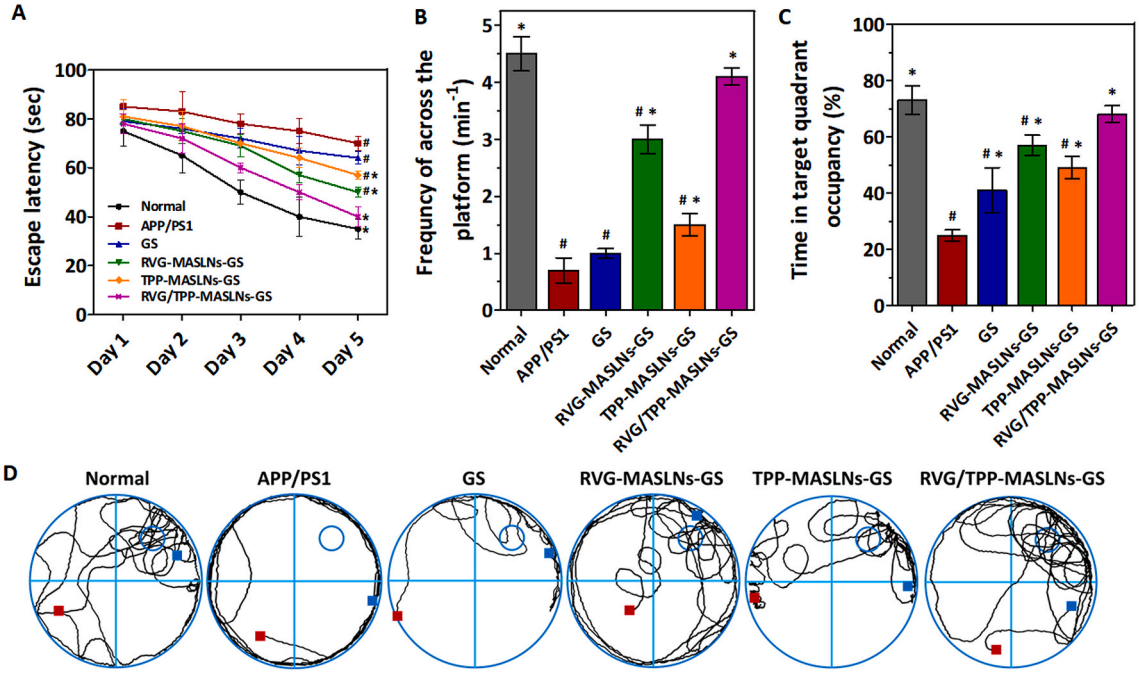

Fig. 6. *In vivo* evaluation of GS-loaded biomimetic nanosystems therapy. (A) Escape latency time in the Morris water maze of APP/PS1 mice. (B) The frequncy of crossing of the removed platform area at the final day. (C) Relative time spent on the target quadrant where the platform was placed before. The data are presented as the means ± SD (n = 20). *p < 0.05 compared with the APP/PS1 group. #p < 0.05 compared with the RVG/TPP-MASLNs-GS group. (D) Representative swimming path tracings of different groups.

the spatial learning ability (Fig. 6D) compared with that of other groups. The above results imply that the anti-AD effect of RVG/TPP-MASLNs-GS is stronger than that of other preparations in the model animals.

3.7. Amelioration of structural neurodegenerative alterations in APP/PS1 transgenic mice by RVG/TPP-MASLNs-GS

Fig. 7A showed the marked neuronal damage (dark purple) in the dentate gyrus of hippocampal region in the APP/PS1 transgenic mice. Administration of GS-loaded formulations slowed the alleviation of degenerative alterations of hippocampal neurons in AD mice to different extent. The trend of hippocampal structural improvement in all treatment groups was consistent with the reverse of the cognitive deficits by the GS-loaded formulations in Fig. 6. In particular, RVG/TPP-MASLNs-GS treatment significantly alleviated neuronal damage, exhibited by the neurons which were morphologically intact and neatly arranged with uniform color (light purple).

3.8. Decreased aβ deposition in APP/PS1 transgenic mice by RVG/TPP-MASLNs-GS

Aβ plaque is one of the key markers of AD. To investigate the inhibitory effect of the GS-loaded biomimetic nanosystems on Aβ deposition *in vivo*, the level of $A\beta_{1\text{-}42}$ was measured by Western blot in APP/PS1 mice hippocampus homogenate (Fig. 7B). The level of $A\beta_{1\text{-}42}$ decreased significantly in APP/PS1 model mice treated with RVG/TPP-MASLNs-GS compared with other formulations. The results confirmed that the observed decreased levels of Aβ in brain were accompanied with learning and memory improvements (Fig. 6).

3.9. Alleviated oxidative stress in APP/PS1 transgenic mice by RVG/TPP-MASLNs-GS

Because oxidative stress could cause the structural and functional damage of neurons, improving the oxidative stress in brain may protect neurons [45]. Previous studies have also shown that ROS-caused oxidative stress not only acts as an inducer but also possesses a sustaining factor in AD [46]. Thus, the levels of MDA and total SOD activity were measured to determine whether GS-loaded biomimetic nanosystems could protect against oxidative stress from ROS in the hippocampus of APP/PS1 mice (Fig. 7C and D). The results of these biomarkers assays showed that the RVG/TPP-MASLNs-GS effectively reduced the lipid peroxidation damage and restored the decreased SOD activity caused by oxidative stress in the hippocampus. The tendency found above agreed with the finding of the cognitive improvement (Fig. 6).

3.10. Prevention of abnormal glial activation and neuro-inflammation by RVG/TPP-MASLNs-GS

Microglia and astrocytes are abundant in the CNS and are essential for brain development and homeostasis. These cells is also a possible contributing factor to neurodegenerative and psychiatric disease. Evidence shows that the neuroinflammation caused by chronic glial activation contribute to neuronal and axonal degeneration, leading the progression of neurodegenerative diseases, including AD [47–49]. Therefore, we further analyzed the effect of RVG/TPP-MASLNs-GS on inflammation related to astrocytic and microglial activation after the MWM test. As shown in Fig. 7E, glial fibrillary acidic protein (GFAP, a biomarker of astrocytes) and ionized calcium binding adaptor molecule-1 (Iba-1, a biomarker of microglia) demonstrated significant higher levels in the APP/PS1 mice, indicating the reactive gliosis. As expected, both GFAP and Iba-1 expressions were significantly decreased in the hippocampus of the APP/PS1 mice treated with RVG/TPP-MASLNs-GS compared with other formulations. Meanwhile, RVG/TPP-MASLNs-GS remarkedly down-regulated the levels of IL-6 (Fig. 7F) and TNF-α (Fig. 7G) in brain of AD mice, consistent with its suppression on glial activation. The results suggested that RVG/TPP-MASLNs-GS could mitigate brain inflammation by improving mitochondrial oxidative stress synergy with the anti-inflammatory effect of GS in APP/PS1 mice.

Overall, the results *in vitro* (Fig. 5) and *in vivo* (Figs. 6 and 7) indicated a markedly neuroprotective effect of RVG/TPP-MASLNs-GS in

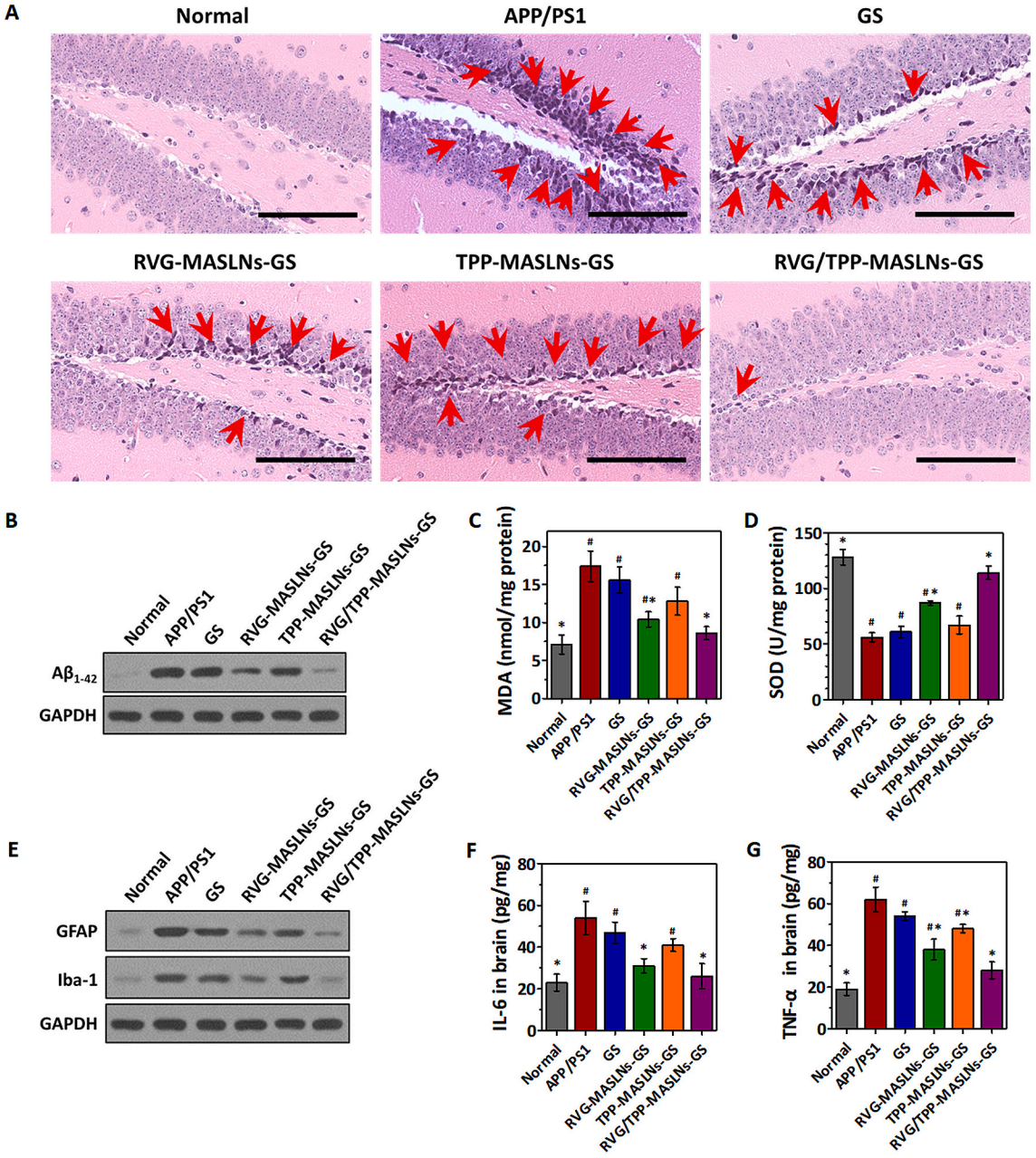

Fig. 7. Neuroprotective effects *in vivo*. (A) H&E staining of hippocampal region of AD mice treated with saline or GS-loaded biomimetic nanosystems (scale bar = 100 μm). Red arrows point to the damaged neurons. (B) Changes of $A\beta_{1\text{-}42}$ levels in the hippocampal area of APP/PS1 mice by western blotting. (C and D) Changes of MDA levels (C) and total SOD activities (D) in the hippocampal area of APP/PS1 mice. (E) Changes of GFAP and Iba-1 expressions in the hippocampal area of APP/PS1 mice by western blotting. (F and G) Changes of IL-6 (F) and TNF-α (G) levels in the hippocampal area of APP/PS1 mice by ELISA. The data are presented as the means ± SD (n = 3). *p < 0.05 compared with the APP/PS1 group. #p < 0.05 compared with the RVG/TPP-MASLNs-GS group.

both Aβ-damaged HT22 neuronal cells and AD model mice. With the proper physiochemical properties (Fig. 1), features of safety (Fig. 2), RES evasion (Fig. 3), BBB permeability and neuronal mitochondial targeting (Fig. 4), the present results provided a proof-of-concept evidence for the GS-encapsulated biomimetic nanosystem as a potential therapeutic candidate for the treatment of oxidative stress-related neurodegenerative disease.

4. Conclusions

In this work, a MA membrane-camouflaged biomimetic drug delivery nanosystem (RVG/TPP-MASLNs) was constructed for efficiently delivering Genistein (GS) into neuronal mitochondria for the treatment of AD. The biological features of the outer MA membranes provided favorable biocompatibility and RES evasion in systemic circulation for the nanosystem. RVG29 and TPP synergistically endowed the formulation with efficient delivery for BBB-crossing and neuronal-targeting, and subsequently reaching the neuronal mitochondria. Although preliminary, the research data of this work collectively suggested the combination of bioactive membranes of macrophages and the functional ligands with suitable polymeric nanoparticles might provide a rational strategy for the design of promising intravenous mitochondria-targeted biomimetic nanosystem in neurodegenerative disease therapy.

CRediT authorship contribution statement

Yang Han: Investigation, Data curation, Writing - original draft. **Chunhong Gao:** Data curation. **Hao Wang:** Data curation. **Jiejie Sun:** Data curation. **Meng Liang:** Data curation. **Ye Feng:** Data curation. **Qianqian Liu:** Data curation. **Shiyao Fu:** Formal analysis. **Lin Cui:** Formal analysis. **Chunsheng Gao:** Formal analysis, Supervision. **Yi Li:** Investigation, Data curation, Formal analysis, Conceptualization, Supervision, Writing - review & editing. **Yang Yang:** Conceptualization, Supervision. **Baoshan Sun:** Supervision.

Declaration of competing interest

The authors declare that they have no conflicts of interests.

Acknowledgments

We are grateful for the financial support from National Science and Technology Major Projects for Major New Drugs Innovation and Development (Grant No. 2018ZX09711003-008-001) and Beijing Natural Science Foundation (Grant No. 7172162).

Appendix A. Supplementary data

Supplementary data related to this article can be found at https://doi.org/10.1016/j.bioactmat.2020.08.017.

References

[1] J. Yao, R.W. Irwin, L.Q. Zhao, J. Nilsen, R.T. Hamilton, R.D. Brinton, Mitochondrial bioenergetic deficit precedes Alzheimer's pathology in female mouse model of Alzheimer's disease, Proc. Natl. Acad. Sci. U.S.A. 106 (34) (2009) 14670–14675.
[2] R.H. Swerdlow, J.M. Burns, S.M. Khan, The Alzheimer's disease mitochondrial cascade hypothesis: progress and perspectives, Biochim. Biophys. Acta (BBA) - Mol. Basis Dis. 1842 (8) (2014) 1219–1231.
[3] R.H. Swerdlow, Mitochondria and mitochondrial cascades in alzheimer's disease, J. Alzheim. Dis. 62 (3) (2018) 1403–1416.
[4] J.E. Selfridge, L.Z. Jianghua Lu, J.H. Lu, R.H. Swerdlow, Role of mitochondrial homeostasis and dynamics in Alzheimer's disease, Neurobiol. Dis. 51 (2013) 3–12.
[5] U. Keil, S. Hauptmann, A. Bonert, I. Scherping, A. Eckert, W.E. Muller, Mitochondrial dysfunction induced by disease relevant A beta PP and tau protein mutations, J. Alzheim. Dis. 9 (2) (2006) 139–146.
[6] D. Pratico, Evidence of oxidative stress in alzheimer's disease brain and antioxidant therapy lights and shadows, Mitochondria Oxidative Stress Neurodegen. Disord. 1147 (2008) 70–78.
[7] C. Pacelli, N. Giguere, M.J. Bourque, M. Levesque, R.S. Slack, L.E. Trudeau, Elevated mitochondrial bioenergetics and axonal arborization size are key contributors to the vulnerability of dopamine neurons, Curr. Biol. 25 (18) (2015) 2349–2360.
[8] H. Du, L. Guo, S.Q. Yan, A.A. Sosunov, G.M. McKhann, S.S. Yan, Early deficits in synaptic mitochondria in an Alzheimer's disease mouse model, Proc. Natl. Acad. Sci. U.S.A. 107 (43) (2010) 18670–18675.
[9] G. Battogtokh, Y.S. Choi, D.S. Kang, S.J. Park, M.S. Shim, K.M. Huh, et al., Mitochondria-targeting drug conjugates for cytotoxic, anti-oxidizing and sensing purposes: current strategies and future perspectives, Acta Pharm. Sin. B 8 (6) (2018) 862–880.
[10] Y. Han, X.Y. Chu, L. Cui, S.Y. Fu, C.S. Gao, Y. Li, et al., Neuronal mitochondria-targeted therapy for Alzheimer's disease by systemic delivery of resveratrol using dual-modified novel biomimetic nanosystems, Drug Deliv. 27 (1) (2020) 502–518.
[11] P. Yang, D.Y. Sheng, Q. Guo, P.Z. Wang, S.T. Xu, K. Qian, et al., Neuronal mitochondria-targeted micelles relieving oxidative stress for delayed progression of Alzheimer's disease, Biomaterials 238 (2020).
[12] H.Y. Zeng, Q. Chen, B.L. Zhao, Genistein ameliorates beta-amyloid peptide (25-35)-induced hippocampal neuronal apoptosis, Free Radical Biol. Med. 36 (2) (2004) 180–188.
[13] Y. Kohara, S. Kawaguchi, R. Kuwahara, Y. Uchida, Y. Oku, K. Yamashita, Genistein improves spatial learning and memory in male rats with elevated glucose level during memory consolidation, Physiol. Behav. 140 (2015) 15–22.
[14] J.G. Wu, J.A. Ge, Y.P. Zhang, Y. Yu, X.Y. Zhang, Solubility of genistein in water, methanol, ethanol, propan-2-ol, 1-butanol, and ethyl acetate from (280 to 333) K, J. Chem. Eng. Data 55 (11) (2010) 5286–5288.
[15] S.Y. Zhou, Y.Z. Hu, B.L. Zhang, Z.H. Teng, H.Q. Gan, Z.F. Yang, et al., Dose-dependent absorption, metabolism, and excretion of genistein in rats, J. Agric. Food Chem. 56 (18) (2008) 8354–8359.
[16] H.J. Kwon, M.Y. Cha, D. Kim, D.K. Kim, M. Soh, K. Shin, et al., Mitochondria-targeting Ceria nanoparticles as antioxidants for alzheimer's disease, ACS Nano 10 (2) (2016) 2860–2870.
[17] N.L. Klyachko, M.J. Haney, Y.L. Zhao, D.S. Manickam, V. Mahajan, P. Suresh, et al., Macrophages offer a paradigm switch for CNS delivery of therapeutic proteins, Nanomedicine 9 (9) (2014) 1403–1422.
[18] A. Parodi, N. Quattrocchi, A.L. van de Ven, C. Chiappini, M. Evangelopoulos, J.O. Martinez, et al., Synthetic nanoparticles functionalized with biomimetic leukocyte membranes possess cell-like functions, Nat. Nanotechnol. 8 (1) (2013) 61–68.
[19] A.V. Kroll, R.H. Fang, Y. Jiang, J.R. Zhou, X.L. Wei, C.L. Yu, et al., Nanoparticulate delivery of cancer cell membrane elicits multiantigenic antitumor immunity, Adv. Mater. 29 (47) (2017).
[20] J.N. Ma, S.Q. Zhang, J. Liu, F.Y. Liu, F. Du, M. Li, et al., Targeted drug delivery to stroke via chemotactic recruitment of nanoparticles coated with membrane of engineered neural stem cells, Small 15 (35) (2019).
[21] R.H. Fang, Y. Jiang, J.C. Fang, L.F. Zhang, Cell membrane-derived nanomaterials for biomedical applications, Biomaterials 128 (2017) 69–83.
[22] Y.L. Zhao, M.J. Haney, N.L. Klyachko, S. Li, S.L. Booth, S.M. Higginbotham, et al., Polyelectrolyte complex optimization for macrophage delivery of redox enzyme nanoparticles, Nanomedicine 6 (1) (2011) 25–42.
[23] A.M. Brynskikh, Y.L. Zhao, R.L. Mosley, S. Li, M.D. Boska, N.L. Klyachko, et al., Macrophage delivery of therapeutic nanozymes in a murine model of Parkinson's disease, Nanomedicine 5 (3) (2010) 379–396.
[24] H.Q. Cao, Z.L. Dan, X.Y. He, Z.W. Zhang, H.J. Yu, Q. Yin, et al., Liposomes coated with isolated macrophage membrane can target lung metastasis of breast cancer, ACS Nano 10 (8) (2016) 7738–7748.
[25] Y. Zhang, K.M. Gai, C. Li, Q. Guo, Q.J. Chen, X. He, et al., Macrophage-membrane-coated nanoparticles for tumor-targeted chemotherapy, Nano Lett. 18 (3) (2018) 1908–1915.
[26] S.Y. Fu, M. Liang, Y.L. Wang, L. Cui, C.H. Gao, X.Y. Chu, et al., Dual-modified novel biomimetic nanocarriers improve targeting and therapeutic efficacy in glioma, ACS Appl. Mater. Interfaces 11 (2) (2019) 1841–1854.
[27] T.E. Park, B. Singh, H. Li, J.Y. Lee, S.K. Kang, Y.J. Choi, et al., Enhanced BBB permeability of osmotically active poly(mannitol-co-PEI) modified with rabies virus glycoprotein via selective stimulation of caveolar endocytosis for RNAi therapeutics in Alzheimer's disease, Biomaterials 38 (2015) 61–71.
[28] G.H. Cui, H.D. Guo, H. Li, Y. Zhai, Z.B. Gong, J. Wu, et al., RVG-modified exosomes derived from mesenchymal stem cells rescue memory deficits by regulating inflammatory responses in a mouse model of Alzheimer's disease, Immun. Ageing 16 (2019).
[29] S. Marrache, S. Dhar, Engineering of blended nanoparticle platform for delivery of mitochondria-acting therapeutics, Proc. Natl. Acad. Sci. U.S.A. 109 (40) (2012) 16288–16293.
[30] W. Baron-Bodo, P. Doceur, M.L. Lefebvre, K. Labroquere, C. Defaye, C. Cambouris, et al., Anti-tumor properties of human-activated macrophages produced in large scale for clinical application, Immunobiology 210 (2–4) (2005) 267–277.
[31] Y. Wang, N. Wang, B. Cai, G.Y. Wang, J. Li, X.X. Piao, In vitro model of the blood-brain barrier established by co-culture of primary cerebral microvascular endothelial and astrocyte cells, Neural Regen. Res. 10 (12) (2015) 2011 +.
[32] J. Liu, L.X. Li, W.Z. Suo, HT22 hippocampal neuronal cell line possesses functional cholinergic properties, Life Sci. 84 (9–10) (2009) 267–271.
[33] T.P. Zhang, H. Wang, Y.H. Ye, X.W. Zhang, B.J. Wu, Micellar emulsions composed of mPEG-PCL/MCT as novel nanocarriers for systemic delivery of genistein: a comparative study with micelles, Int. J. Nanomed. 10 (2015) 6175–6184.
[34] Q. Wang, T.T. Liu, Y. Fu, K. Wang, X.G. Yang, Vanadium compounds discriminate hepatoma and normal hepatic cells by differential regulation of reactive oxygen species, J. Biol. Inorg. Chem. 15 (7) (2010) 1087–1097.
[35] N.V. Soucy, H.D. Parkinson, M.A. Sochaski, S.J. Borghoff, Kinetics of genistein and its conjugated metabolites in pregnant Sprague-Dawley rats following single and repeated genistein administration, Toxicol. Sci. 90 (1) (2006) 230–240.
[36] Y. Omidi, L. Campbell, J. Barar, D. Connell, S. Akhtar, M. Gumbleton, Evaluation of the immortalised mouse brain capillary endothelial cell line, b.End3, as an in vitro blood-brain barrier model for drug uptake and transport studies, Brain Res. 990 (1–2) (2003) 95–112.
[37] L. Yao, X. Gu, Q.X. Song, X.L. Wang, M. Huang, M. Hu, et al., Nanoformulated alpha-mangostin ameliorates Alzheimer's disease neuropathology by elevating LDLR expression and accelerating amyloid-beta clearance, J. Contr. Release 226 (2016) 1–14.
[38] Z.X. Zhao, S.Y. Gao, J.C. Wang, C.J. Chen, E.Y. Zhao, W.J. Hou, et al., Self-assembly nanomicelles based on cationic mPEG-PLA-b-Polyarginine(R-15) triblock copolymer for siRNA delivery, Biomaterials 33 (28) (2012) 6793–6807.
[39] G.M. Baer, J.H. Shaddock, R. Quirion, T.V. Dam, T.L. Lentz, Rabies susceptibility and acetylcholine-receptor, Lancet 335 (8690) (1990) 664–665.
[40] P. Kumar, H.Q. Wu, J.L. McBride, K.E. Jung, M.H. Kim, B.L. Davidson, et al., Transvascular delivery of small interfering RNA to the central nervous system, Nature 448 (7149) (2007) 39–43.
[41] S. Biswas, N.S. Dodwadkar, P.P. Deshpande, V.P. Torchilin, Liposomes loaded with paclitaxel and modified with novel triphenylphosphonium-PEG-PE conjugate possess low toxicity, target mitochondria and demonstrate enhanced antitumor effects in vitro and in vivo, J. Contr. Release 159 (3) (2012) 393–402.
[42] J. Wang, G.J. Chen, Mitochondria as a therapeutic target in Alzheimer's disease, Genes Dis. 3 (3) (2016) 220–227.
[43] Y.S. Qian, L.X. Cao, T. Guan, L. Chen, H.B. Xin, Y.N. Li, et al., Protection by genistein on cortical neurons against oxidative stress injury via inhibition of NF-kappaB, JNK and ERK signaling pathway, Pharm. Biol. 53 (8) (2015) 1124–1132.
[44] G.L. Zhang, W.G. Zhang, Y. Du, L. Yao, H. Sun, R. Zhang, et al., Edaravone ameliorates oxidative damage associated with A beta 25-35 treatment in PC12 cells, J.

Mol. Neurosci. 50 (3) (2013) 494–503.
[45] E. Verdin, M.D. Hirschey, L.W.S. Finley, M.C. Haigis, Sirtuin regulation of mitochondria: energy production, apoptosis, and signaling, Trends Biochem. Sci. 35 (12) (2010) 669–675.
[46] R.H. Swerdlow, S.M. Khan, A "mitochondrial cascade hypthesis" for sporadic Alzheimer's disease, Med. Hypotheses 63 (1) (2004) 8–20.
[47] S.D. Mhatre, C.A. Tsai, A.J. Rubin, M.L. James, K.I. Andreasson, Microglial malfunction: the third rail in the development of alzheimer's disease, Trends Neurosci. 38 (10) (2015) 621–636.
[48] H. Asai, S. Ikezu, S. Tsunoda, M. Medalla, J. Luebke, T. Haydar, et al., Depletion of microglia and inhibition of exosome synthesis halt tau propagation, Nat. Neurosci. 18 (11) (2015) 1584–1593.
[49] A.D. Greenhalgh, S. David, F.C. Bennett, Immune cell regulation of glia during CNS injury and disease, Nat. Rev. Neurosci. 21 (3) (2020) 139–152.
[50] E. Hinde, K. Thammasiraphop, H.T.T. Duong, J. Yeow, B. Karagoz, C. Boyer, et al., Pair correlation rnicroscopy reveals the role of nanoparticle shape in intracellular transport and site of drug release, Nat. Nanotechnol. 12 (1) (2017) 81–89.
[51] S. Marrache, S. Dhar, Engineering of blended nanoparticle platform for delivery of mitochondria-acting therapeutics, Proc. Natl. Acad. Sci. U.S.A. 109 (40) (2012) 16288–16293.